Optical properties of highly n-doped germanium obtained by in-situ doping and laser annealing

J Frigerio[1], A Ballabio[1], K Gallacher[2], V Giliberti[3], L Baldassarre[3], R Millar[2], R Milazzo[4], L Maiolo[5], A Minotti[5], F Bottegoni[6], P Biagioni[6], D Paul[2], M Ortolani[3], A Pecora[5], E Napolitani[4] and G Isella[1]

[1] L-NESS, Dipartimento di Fisica, Politecnico di Milano,Polo di Como, Via Anzani 42, I-22100 Como, Italy

[2] School of Engineering, University of Glasgow, Rankine Building,Oakfield Avenue, Glasgow G12 8LT, United Kingdom

[3] Dipartimento di Fisica, Sapienza Università di Roma, Piazzale Aldo Moro 5, I-00185 Rome, Italy

[4] Dipartimento di Fisica e Astronomia, Università di Padova and CNR-IMM Matis, Via Marzolo 8, I-35131 Padova, Italy

[5] CNR-IMM, Via del Fosso del Cavaliere 100, 00133 Roma, Italy

6 Dipartimento di Fisica, Politecnico di Milano, piazza Leonardo da Vinci 32, I-20133 Milano, Italy

E-mail: jacopo.frigerio@polimi.it

Abstract: High n-type doping in germanium is essential for many electronic and optoelectronic applications especially for high performance Ohmic contacts, lasing and mid-infrared plasmonics. We report on the combination of in-situ doping and excimer laser annealing to improve the activation of phosphorous in germanium. An activated n-doping concentration of 8.8×10^{19} cm^{-3} has been achieved starting from an incorporated phosphorous concentration of 1.1×10^{20} cm^{-3}. Infrared reflectivity data fitted with a multi-layer Drude model indicate good uniformity over a 350 nm thick layer. Photoluminescence demonstrates clear bandgap narrowing and an increased ratio of direct to indirect bandgap emission confirming the high doping densities achieved.

1. Introduction

Heavily doped n-type germanium is attracting an increasing interest driven by its potential applications in microelectronics, photonics, spintronics and mid-infrared (mid-IR) plasmonics. Ge based CMOS [1] is under investigation for end-of-the-roadmap electronic applications, where low resistivity n-type Ohmic contacts [2] and good n^+-p junctions [3] are mandatory in order to take full advantage of the superior electron mobility of Ge as compared to Si. Doping [4,5] is the key tool, together with tensile strain [6-8], to engineer the band structure of germanium for the development of an efficient Ge-on-Si laser. Recently n-type Ge has been recognized as a promising material for the realization of electrically driven spintronic devices thanks to the long electron spin lifetime and the large spin accumulation [9,10]. Moreover Ge has been identified as a key-material for the realization of mid-IR waveguides [11,12] due to the absence of strong intraband transitions

in the 1.9-14 μm wavelength range. Recently it has been demonstrated that, by doping germanium in the low 10^{19} cm^{-3} range, it is possible to tune its plasma wavelength to around 10 μm (plasma frequency $\omega_p \approx 1000$ cm^{-1}) [13] thus enabling mid-IR plasmon enhanced sensing [14-15]. In addition, the compatibility of germanium with standard silicon foundry processes can boost the pervasive exploitation of plasmonic effects in the infrared. In order to fully exploit the potential of Ge-on-Si plasmonics, however, a doping density approaching 10^{20} cm^{-3} over a uniform doping profile of the order of a few electromagnetic skin depths, i.e. approximately 300-500 nm, would be desirable in order to cover the whole relevant fingerprint region in the mid-infrared. Achieving a uniform activation profile is extremely relevant for mid-IR sensing since layers with different electron concentrations would lead to a variation of the plasma frequency within the Ge layer and a consequent smearing-out of all resonant effects. Furthermore, the thickness of such highly-doped layer should be sufficient to clearly determine the plasma frequency ω_p separating the frequency region ($\omega > \omega_p$) where the semiconductor is highly transparent, from the frequency region ($\omega < \omega_p$) where a metallic behavior is observed. Phosphorous doping of Ge-on-Si epilayers performed at temperatures around T≈500-600 °C and employing GeH_4 and PH_3 as precursor gases typically results in an activated doping density $n_e \approx 2\times10^{19}$ cm^{-3} [16,17]. Deposition at lower temperatures, which requires the use of specialized precursor gases, resulted in an increased activation ($n_e \approx$ 6-7×10^{19} cm^{-3}) [18-20] even though a much higher dopant atom incorporation of N_D≈1-2×$10^{20}$$cm^{-3}$ was observed in these cases. Electron densities as high as $n_e \approx 2.2\times10^{20}$ cm^{-3} have been obtained by in-situ doping, although on layers of thickness below 100 nm, by using a combination of molecular beam epitaxy (MBE) for Ge deposition and low temperature exposure to PH_3, which leads to the formation of a mono-atomic P layers, subsequently incorporated [21] by means of Ge regrowth and thermal treatments. The implementation of such atomic-layer doping approach in a CVD reactor has been only partially successful, possibly because of the critical role played by hydrogen adsorbed on the Ge surface during PH_3 exposure. A combination of P-implantation and flash-lamp-annealing has also been used to achieve an active carrier concentration of $n_e \approx 2.2\times10^{20}$ cm^{-3} however the implantation depth limits the thickness of the doped layer to approximately 150nm [22]. An alternative approach to increase the active doping concentration is laser thermal annealing (LTA). In the LTA process one or more laser pulses are used to melt the ion-implanted or in-situ doped semiconductor. The subsequent fast, out of equilibrium recrystallization process, enhances the substitutional incorporation of dopants in the material. Moreover, by using pulses in the nanoseconds range, dopant diffusion is limited within the molten region and a box-like doping profile can be obtained. LTA has been successfully employed to achieve a doping activation above 10^{20} cm^{-3} in implanted bulk [23,24] Ge and in in-situ doped Ge-on-Si epilayers [25]. In both cases, however, only electrical measurements have been performed to characterize the highly doped region, which is limited to a thickness of ~ 100 nm. In this work we have investigated the use of LTA to obtain uniform active doping levels close to 10^{20} cm^{-3} in 500 nm thick, in-situ doped Ge-on-Si. The structural properties of the samples have been investigated by atomic force microscopy (AFM), secondary ion mass spectrometry (SIMS) and μ-Raman spectroscopy and the optical properties have been explored, in the mid-IR, by means of infrared reflectometry and, in the near-IR, by means of photoluminescence spectroscopy. The measured plasma frequency of $\omega_p \approx 1850$ cm^{-1} makes these epilayers

suitable for plasmon-enhanced sensing of most organic substances, as the important carbonyl-carboxyl fingerprint region at 1600-1750 cm^{-1} is now fully covered if compared to previous doped semiconductor plasmonic devices [14,26]. On a different perspective, band gap narrowing and the residual tensile strain of ≈ 0.38%, induced by LTA are seen to red-shift the direct bandgap PL to ≈ 1.8 μm making this doping procedure attractive for integrated photonics applications [27,28].

2. Sample preparation

The sample was grown by Low-Energy Plasma-Enhanced Chemical Vapor Deposition (LEPECVD) [29] and it consists of a ≈ 500 nm thick Ge layer deposited at 500 °C at a rate of 1 nm/s with a GeH_4 flux of 20 sccm. The doping was obtained by adding 0.35 sccm of PH_3 during the growth. LTA was performed in vacuum by using a Lambda Physik LPX 305 XeCl excimer laser (λ=308 nm, 28 ns pulse duration) with an energy density of 1 J/cm^2 covering a sample area of 5×5 mm^2 in total by raster scanning the sample with 1 mm steps and firing a total of 25 laser shots. In this work we will compare the optical properties of the "as grown" Ge-on-Si epilayer with those of 100×100 μm^2 regions of the same sample that underwent the laser annealing process.

3. Structural characterization

Two 20×20 μm^2 atomic force microscopy (AFM) scans of the Ge-on-Si sample before and after the LTA are reported in figure 1. The as-grown sample features a smooth surface with an RMS roughness of about 0.5 nm.

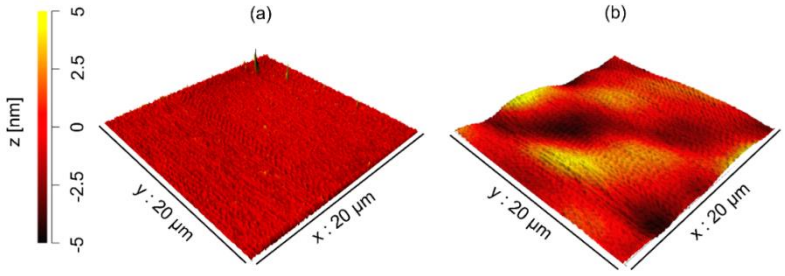

Figure 1. 20×20 μm^2 AFM scans of the sample before (a) and after (b) the LTA process.

After LTA, the AFM scan reveals surface undulations due to re-crystallization. These undulations have a periodicity of ≈10 μm and an average vertical amplitude of about 5 nm. The chemical P concentration N_D and the electron density n_e have been measured by secondary ion mass spectrometry (SIMS) and infrared reflectometry, respectively. SIMS measurements have been performed by using a CAMECA ims-4f mass

spectrometer. An O_2^+ ion beam with an accelerating voltage of 3 keV, rastered over a 250×250 μm^2 area, was used for sputtering, while collecting $^{31}P^{16}O^+$ secondary ions. The calibration of the P concentration was performed by measuring a Ge standard with known P areal density with an accuracy of ±15%. The measurement reproducibility is ±5%. The effects of laser annealing on the P incorporation profile are shown in figure 2. The incorporated dopant concentration in the as-grown sample has an almost constant value of about 1.1×10^{20} cm^{-3} over 450 nm. Such P incorporation is almost ten times higher than the one obtained in thermal CVD for similar growth temperatures and PH_3/GeH_4 ratios [19] pointing out the key-role played by the plasma-enhanced deposition. Moreover, by comparing the SIMS profiles before and after irradiation with a 1 J/cm^2 pulse, it can be noticed that only a very slight redistribution of dopants takes place, in agreement with the absence of redistribution expected from Fick's law in the case of zero concentration gradient and with reflecting boundary conditions at the surface (i.e. no P surface segregation or out-diffusion).

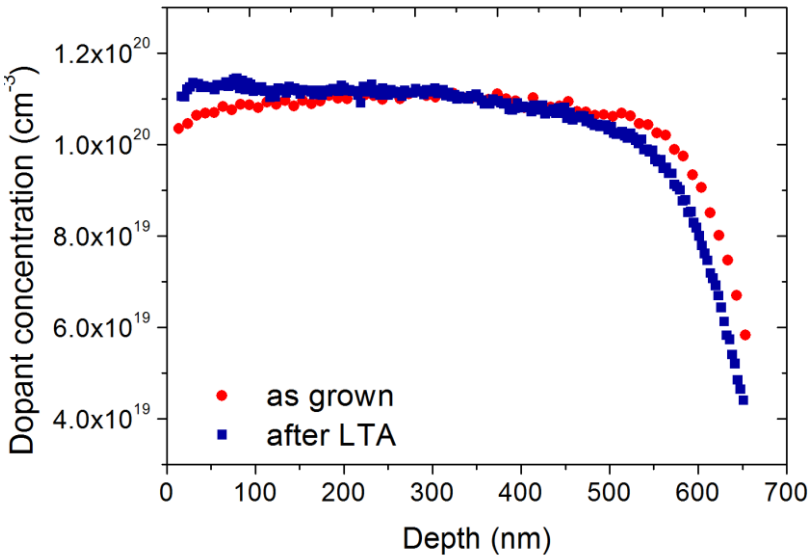

Figure 2. The SIMS profiles of the sample before (red circles) and after (blue squares) the LTA process.

4. Optical characterization

The frequency-dependent absolute normal-incidence reflectivity was measured in the 600-6000 cm^{-1} (1.6–17 μm wavelength) range with an infrared microscope (Bruker Hyperion) and a nitrogen-cooled photovoltaic detector (Infrared Associates HgCdTe) coupled to a Bruker IFS 66v Fourier-Transform spectrometer (FTIR). The knife-edge aperture of the microscope was kept at 100×100 μm^2 while scanning the 5×5 mm^2 area subject to LTA hence obtaining an active-carrier concentration map. The reflectivity spectrum measured at the locations in the center of different LTA spots was approximately the same. The active carrier density is obtained by fitting the absolute IR reflectance of the film with a multi-layer Drude model where the number of layers with different dielectric function is kept at a minimum, but still left as a free parameter of the fitting routine, as explained in details in [13]. The extraction of n_e from IR data only relies on the knowledge of the

effective mass $m^* \approx 0.12$ and the IR low-frequency dielectric constant of Ge $\varepsilon_\infty \approx 16$, which are known with a much higher accuracy than the Hall factor, the specific Ohmic contact resistivity or the thickness of the heavily doped layer, all affecting the analysis of electrical measurements [18]. The reflectivity spectra of the sample before and after the LTA process are reported in figure 3.

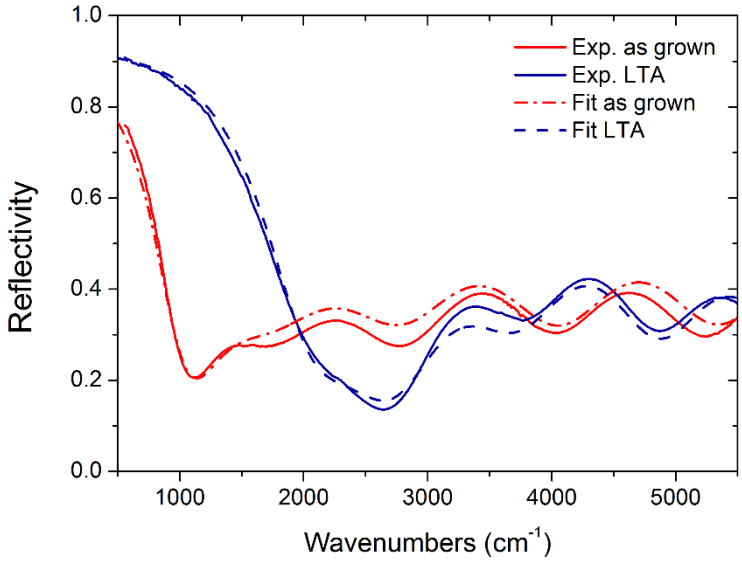

Figure 3. The reflectivity spectra of the as grown sample (red line) and of the LTA treated sample (blue line). The multi-layer Drude fitting of both spectra are reported as a red dashed line and as a dash-dotted blue line respectively.

By fitting the multi-layer Drude model to the spectra, we found that the as-grown sample has a homogeneous dielectric function throughout its thickness of 500 nm, while a multi-layer Drude model was needed to reproduce the sample subject to LTA, with at least two layers required of thickness 350 nm and 150 nm respectively. The best-fit active carrier concentration increased from $n_e = 2.1 \pm 0.2 \times 10^{19}$ cm^{-3} for the as grown sample to $n_e = 8.8 \pm 0.9 \times 10^{19}$ cm^{-3} in the top 350 nm layer after the LTA treatment. The latter value is compatible, within errors, with the chemical P concentration measured by SIMS, indicating that full P activation has been achieved thanks to LTA processing. The second and deeper layer with thickness 150 nm had $n_e = 3 \pm 1 \times 10^{19}$ cm^{-3}, suggesting that the bottom part of the Ge film did not experience melting and recrystallization as the top part. We stress that the multi-layer Drude fit does not indicate the presence of a physical interface at a depth of 350 nm, rather it provides an average description. The use of more layers or of a doping-dependent profile would probably provide a more accurate description, at the expense of the simplicity of the model. The high activation achieved using LTA is confirmed by photoluminescence (PL) measurements. PL spectra have been acquired at room temperature by using a Bruker Vertex 70 FTIR system. The samples were optically pumped with a continuous wave frequency doubled Nd:YAG laser operating at 532 nm wavelength. The laser illuminates the sample through an aperture in a parabolic mirror. The sample

emission is collected by this mirror, which then couples the emission into the internal Michelson interferometer of the FTIR system before detection by an extended InGaAs camera [30]. In order to disentangle band-gap narrowing (BGN) effects due to the activated doping from those related to strain, the strain-state of the as grown and annealed samples needs to be characterized. To this purpose, the residual strain in the as-grown sample has been measured by means of high-resolution X-ray diffraction (HR-XRD) obtaining a very small in plane tensile strain of $\varepsilon_{\parallel} \approx +5\times10^{-4}$. Ge-on-Si typically exhibits a residual tensile strain, induced by the thermal expansion coefficient mismatch between Ge and Si developing during cool-down from the growth (or annealing) temperature to room-temperature, consistently with the relatively low deposition temperature employed in our work, a negligible tensile strain is found in the as-grown sample. Strain effects related to the dopant atoms incorporation are expected to be very weak (few 10^{-5} at the most) in the case of phosphorous [31] and can therefore be neglected. The small dimensions of the laser annealed area did not allow a reliable HR-XRD characterization of the laser annealed sample, therefore a μ-Raman set-up was used to compare the as-grown and annealed areas. A comparison of the two Raman spectra is shown in figure 4. By using a biaxial strain shift coefficient [32] b_{biax}=-416 cm^{-1} a significant residual tensile strain of $\varepsilon_{\parallel} \approx +3.7\times10^{-3}$ is obtained from the Raman shift with respect to the as grown sample. Tensile strain is not observed in laser annealed bulk Ge [23] while it has already been reported in Ge-on-Si epilayers [27]: this suggests that, also in the case of laser annealed epilayers, tensile strains develops due to the thermal expansion coefficient mismatch between Ge and Si. It is worth noticing that the measured strain exceeds the calculated maximum tensile strain $\varepsilon_{\parallel}\approx+2.8\times10^{-3}$ achievable for the case of Ge-on-Si heterostructure cooling down from the Ge melting temperature (T_H = 937°C) to room temperature [33]. Such limiting value of $\varepsilon_{\parallel}\approx+2.8\times10^{-3}$ is obtained only in the case that both epilayer and substrate cool down from the same initial temperature T_H. If we allow the substrate to reach a maximum temperature lower than T_H, as is the case for the highly non-uniform temperature distribution attained by laser annealing, strain values larger than 2.8×10^{-3} are indeed achievable.

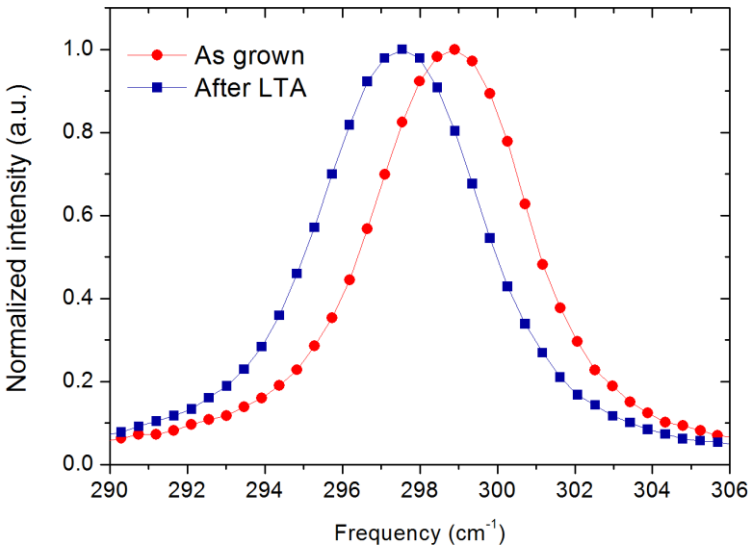

Figure 4. Raman spectra of the as grown sample (red circles) and after the LTA (blue squares).

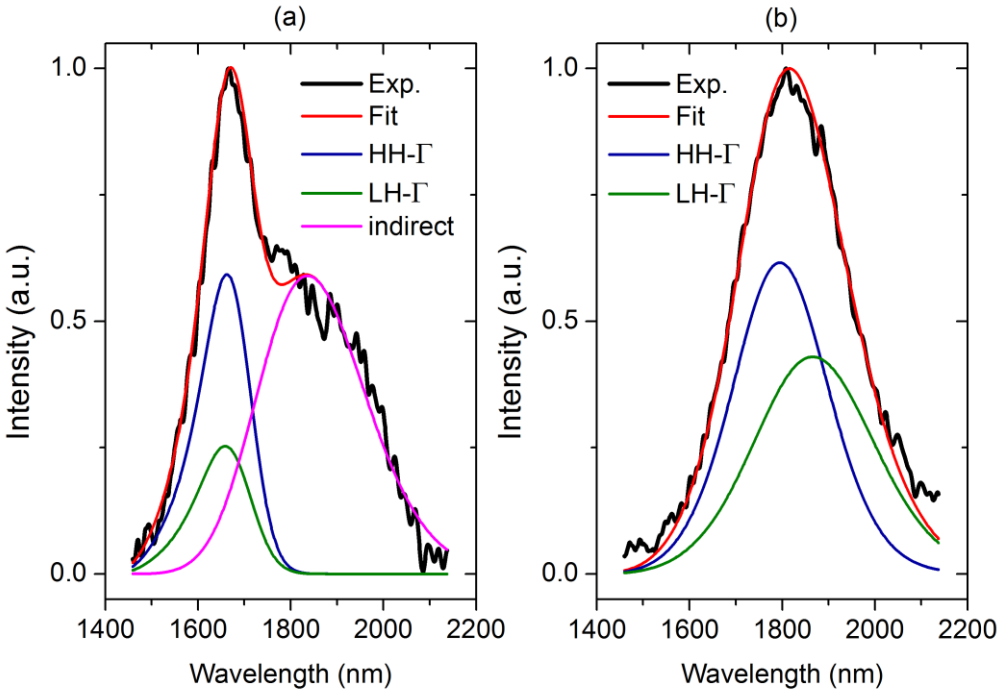

Figure 5. Normalized PL intensity as a function of the wavelength from an as-grown region of the Ge-on-Si epilayer (a), and of the LTA treated region (b). The PL lineshape has been analyzed considering the recombination from Γ-heavy holes (blue line), Γ- light holes (green line) and indirect radiative transitions (magenta lines).

The PL spectrum of the as grown epilayer (see figure 5a) is dominated by a sharp peak at $\lambda \approx 1.67$ µm, which can be attributed to direct-gap recombination. As typically observed in Ge-on-Si epilayers the indirect related PL (the shoulder extending in the range ≈ 1.8 – 2.1 µm) is relatively weak due to the inherently low radiative recombination rate of phonon-assisted transitions and the stronger impact of non-radiative recombination on L-valley electrons, as compared to Γ-valley electrons [34]. The broadening of the indirect-gap peak [35] is consistent with the relatively high doping level measured by IR reflectometry ($n_e = 2.1\times10^{19}$ cm^{-3}) for this sample, which corresponds to a Fermi level located ~0.03 eV above the L-valley minima. The indirect related PL was modeled with a Gaussian profile (magenta line in figure. 5a) with a FWHM of ~0.18 eV and subtracted from the PL spectra to better analyze the direct-gap related lineshape. Camacho et al. [36] have proposed a linear phenomenological expression for the estimation of the active carrier density from the peak position of the direct-gap PL, however, it must be noticed that such expression contains a constant term, accounting for the strain-induced BGN, which limits its applicability to Ge-on-Si epilayers with a residual strain comparable to that reported by Camacho et al. ($\varepsilon_{\parallel}\approx+2.5\times10^{-3}$). For this reason the direct-gap PL spectra have been fitted with a generalized van Roosbroeck–Shockley expression following the procedure reported in [37,38] and including the strain-induced BGN and related removal of the HH-LH degeneracy. In this way the contribution to BGN solely due to doping effects can be estimated. As already mentioned, the as-grown sample features a negligible strain $\varepsilon \approx +5\times10^{-4}$, yet strain effects have been included in our modelling with the aim of applying an equal fitting procedure to as-grown and laser annealed samples. The energy of the direct bandgap between

the Γ-valley and HH states obtained from the PL data fitting is $E^d_{HH} \approx 0.75$ eV. This is in good agreement with the value calculated considering a bandgap narrowing (BGN) given by the expression $\Delta E_{BGN} = 8.33 \times 10^{-3}\sqrt{n_e/10^{18}}$ (eV), which describes doping-induced effects at the direct and indirect bandgap of Ge [37]. After laser annealing (figure 5b) the direct bandgap PL peak is observed to shift to longer wavelengths while the indirect bandgap contribution to the spectra is strongly reduced. In this case, therefore, the lineshape analysis was performed considering direct bandgap transitions only and a tensile strain $\varepsilon \approx 3.7\times10^{-3}$. In the case of figure 5b, the direct bandgaps obtained from the PL data fitting are E^d_{HH} (E^d_{LH})≈0.69 (0.66) eV. By using the deformation potential and unstrained bandgaps reported in Table 1, the strain contribution to the bandgap reduction has been calculated to isolate the BGN contribution and eventually estimate the active carrier density. An active carrier density $n_e \approx 8.9 \times 10^{19}$ cm^{-3} has been obtained after laser annealing, in good agreement with IR reflectometry results. At such doping and strain levels, the Fermi level lays ≈15 meV below the Γ-valley and the relative population ratio between the Γ and L valley electrons is ~3×10^{-3} i.e. an order of magnitude higher than the one expected in the as-grown epilayer..

Table1: Parameters used for PL lineshape fitting.

a^{Γ} (eV)	a^{L} (eV)	b (eV)	E_g^{Γ} (eV)	E_g^{L} (eV)
-9.47[a]	-3.6[b]	-1.88[c]	0.80	0.66

[a] [38]

[b] [39]

[c] [40]

5. Conclusions

In conclusion, we have investigated the capability of the combined use of excimer laser annealing and in-situ doping to achieve high doping levels in Ge-on-Si epilayers. An active doping level of 8.8×10^{19} cm^{-3} fairly constant over a thickness of 350 nm has been measured by infrared spectroscopy. The absolute reflectance spectra of the LTA treated sample shows a clear transition between the frequency region where the semiconductor is transparent, from the frequency region where a metallic behavior is observed, with a plasma frequency approximately located at 1850 cm^{-1} (∼5.4 μm wavelength). This result paves the way for the realization of Ge-on-Si based plasmon-enhanced sensors covering the whole carbonyl-carboxyl fingerprint region. Moreover, PL spectra confirm the high doping densities achieved in these samples. The significant increase of the relative population ratio between the Γ and L valleys suggest the relevance of such epilayers for the realization of efficient Ge-on-Si laser sources.

Acknowledgments

The research leading to these results has received funding from the European Union's Seventh Framework Programme under grant agreement no. 613055. The authors would like to thank J. Menéndez for his support in PL data analysis.

References

[1] Pillarisetty R 2011 *Nature* **479**, 324.

[2] Gallacher K, Velha P, Paul D J, MacLaren I, Myronov M and Leadley D R 2012 *Appl. Phys. Lett*. **100** ,022113.

[3] Jamil M, Mantey J, Onyegam E U, Carpenter G D, Tutuc E and Banerjee S K 2011 *IEEE Elec. Dev. Lett*. **32**, 1203.

[4] Liu J, Sun X, Camacho-Aguilera R , Kimerlingh L C and Michel J 2010 *Opt. Lett*. **35**, 679.

[5] Camacho-Aguilera R, Cai Y, Patel N, Bessette J T, Romagnoli M, Kimerlingh L C and Michel J 2012 *Opt. Expr*. **20**, 11316.

[6] Suess M J, Geiger R, Minamisawa R, Schiefler G, Frigerio J, Chrastina D, Isella G, Spolenak R, Faist J and Sigg H 2013 *Nat. Photon*. **6**, 466.

[7] G. Capellini et al 2013 *J. Appl. Phys*. **113**, 013513.

[8] R W Millar, Gallacher K, Frigerio J, Ballabio A, Bashir A, MacLaren I, Isella G and Paul D J 2016 *Opt. Expr*. **24** 4365.

[9] Bottegoni F, Zucchetti C, Dal Conte S, Frigerio J, Carpene E, Vergnaud C, Jamet M, Isella G, Ciccacci F, Cerullo G and Finazzi M 2017 *Phys. Rev. Lett*. 118, 167402.

[10] Ferrari A, Bottegoni F, Isella G, Cecchi S and Ciccacci F 2013 *Phys. Rev. B* 88, 115209.

[11] Soref R 2012 *Nat. Photon.* **4**, 495.

[12] Chang Y C, Paeder V, Hvozdara L, Hartmann J M, and Herzig H P 2012 *Opt. Lett*. **37**, 2883.

[13] Frigerio J et al 2016 *Phys. Rev. B* **94**, 085202.

[14] Baldassarre L, Sakat E, Frigerio J, Samarelli A, Gallacher K, Calandrini E, Isella G, Paul D J, Ortolani M, and Biagioni P 2015 *Nano Lett.* **15**, 7225.

[15] Biagioni P et al 2015 *J. Nanophoton*. **9**, 093789.

[16] Cai Y, Camacho-Aguilera R, Bessette J T, Kimerling L C, and Michel J 2012 *J. Appl. Phys*. **112**, 034509.

[17] Carroll L, Friedli P, Neuenschwander S, Sigg H, Cecchi S, Isa F, Chrastina D, Isella G, Fedoryshyn Y, and Faist J 2012 *Phys. Rev. Lett*. **109**, 057402.

[18] Xu C, Senaratne C L, Kouvetakis J, and Menéndez J 2014 *Appl. Phys. Lett*. **105**, 232103.

[19] Shimura Y, Srinivasan S A, Van Thourhout D, Van Deun R, Pantouvaki M, Van Campenhout J and Loo R 2016 *Thin Solid Films* **602**, 56.

[20] Moriyama Y, Kamimuta Y, Kamata Y, Ikeda K, Sakai A, and Tezuka T 2014 *Appl. Phys. Expr*. **7**, 106501.

[21] Scappucci G, Capellini G, Lee W T C and Simmons M Y 2009 *Appl. Phys. Lett*. **94**, 162106.

[22] Prucnal S et al 2016 *Sci. Rep*. **6**, 27643.

[23] Milazzo R et al 2014 *J. Appl. Phys*. **115**, 053501

[24] Heo S, Baek S, Lee D, Hasan M, Jung H, Lee J, and Hwang H 2006 *Electrochem. Solid-State Lett*. **9**, G136.

[25] Huang S H, Lu F L, Huang W L, Huang C H, and Liu C W 2015 *IEEE Electron Device Lett*. **36**, 1114.

[26] Law S, Yu L, Rosenberg A and Wasserman D 2013 *Nano Lett.* **13**, 4569.

[27] Wen H and Bellotti E 2015 *Phys. Rev. B* **91**, 035307.

[28] Pizzi G, Virgilio M and Grosso G 2012 *Nanotechnology* **21**, 55202.

[29] Isella G, Chrastina D, Rössner B, Hackbarth T, Herzog H J, König U, Von Känel H 2004 *Solid State Electron*. **48**, 1317.

[30] Millar R W, Gallacher K, Samarelli A, Frigerio J, Chrastina D, Isella G, Dieing T and Paul D J 2015 *Optics Expr*. **23**, 18193

[31] Xu C, Senaratne C L, Kouvetakis J and Menéndez J 2016 *Phys. Rev. B* **93**, 041201.

[32] Fang Y Y, Tolle J, Roucka R, Chizmeshya A V G, Kouvetakis J, D'Costa V R, and Menéndez J 2007 *Appl. Phys. Lett*. **90**, 61915.

[33] Capellini G, De Seta M, Zaumseil P, Kozlowski G and Schroeder T 2012 *J. Appl. Phys*. **111**, 73518.

[34] Grzybowski G, Roucka R, Mathews J, Jiang L, Beeler R, Kouvetakis J and Menéndez J 2011 *Phys. Rev. B* **84**, 205307.

[35] Wagner J 1985 *Solid. State. Electron*. **28**, 25.

[36] Camacho-Aguilera R, Han Z, Cai Y, Kimerling L C and Michel J 2013 *Appl. Phys. Lett*. **102**, 152106.

[37] Jiang L, Gallagher J D, Senaratne C L, Aoki T, Mathews J, Kouvetakis J and Menéndez J 2014 *Semicond. Sci. Technol.* 29, 115028.

[38] Xu C, Gallagher J D, Wallace P M, Senaratne C L, Sims P, Menéndez J. and Kouvetakis J 2015 *Semicond. Sci. Technol*. 30, 105028.

[39] Teherani J, Chern W, Antoniadis D, Hoyt J, Ruiz L, Poweleit C and Menéndez J 2012 Phys. Rev. B **85**, 205308.

[40] Ahmad C N and Adams A R 1986 *Phys. Rev. B* **34**, 2319.

[41] Liu J, Cannon D, Wada K, Ishikawa Y, Danielson D, Jongthammanurak S, Michel J and Kimerling L 2004 *Phys. Rev. B* **70**, 155309.